Slowing and Speeding Molecular Beams by Means of a Rapidly Rotating Source†

Manish Gupta‡ and Dudley Herschbach*

Department of Chemistry and Chemical Biology, Harvard University, Cambridge, Massachusetts 02138

Received: July 25, 2000; In Final Form: October 17, 2000

Mounting a molecular beam source near the tip of a hollow high-speed rotor provides a means to shift the velocity distribution of the beam downward or upward over a wide range. We describe the construction of such a device and experiments and model calculations characterizing its operation, for both supersonic and effusive beams of rare gases, O_2, CH_3F, and SF_6. For example, the flow velocity of a rotating supersonic beam of O_2 was accelerated to above 1000 m/s (corresponding to a kinetic energy of 2200 K and deBroglie wavelength of 0.1 Å) and decelerated (when seeded in Xe) to below 70 m/s (corresponding to a kinetic energy below 10 K and deBroglie wavelength of nearly 2 Å). With improvements in prospect, the rotating beam source offers a versatile and relatively simple way to enhance techniques for manipulating molecular trajectories.

Introduction

Eighty years ago, Otto Stern began the saga of molecular beams in physics and chemistry with an experiment to test the Maxwell−Boltzmann velocity distribution.[1] His apparatus was mounted within a rotating cylinder (turning at the sedate peripheral velocity of 15 m/s), the ancestor of many devices since used for velocity analysis. The first use of rotation as a means to accelerate molecules did not come until the 1950s, when Philip Moon used a high-speed rotor to swat molecules in one of the first successful crossed beam studies of a chemical reaction.[2] In later work, he considered trying effusion from a hollow rotor.[3] However, Moon opted to continue with swatting as a simpler means to produce intense fast pulsed beams, attaining peripheral velocities as high as 1.7 km/s.[4] We have undertaken development of a hollow rotor source operable in the supersonic regime. Thereby, the ability of a supersonic expansion to drastically cool molecular motions with respect to its flow velocity can be coupled with the ability to shift that flow velocity downward or upward in the laboratory frame.[5]

A chief motivation for developing such a device is to enhance the means for influencing molecular trajectories by interaction with external fields,[6] particularly laser fields.[7,8] All such techniques become most effective for molecules with low translational kinetic energy. Most enticing is the prospect for spatial trapping of molecules,[9] which requires the kinetic energy be reduced below ~1 K. Once trapped in sufficient quantity, molecules may be cooled much further by evaporative cooling, perhaps to the microkelvin range.[10] This would endow them with deBroglie wavelengths that are large compared with the molecular diameters and thus enable study of chemistry with "nanowave-matter". Recently, two elegant means of slowing molecules have achieved trapping. One method[11] employs collisional relaxation by ^{3}He buffer gas, maintained by a dilution refrigerator at about 0.3 K. The other method[12] decelerates polar molecules by means of multiple stages of time-varying electric field gradients, bringing them down to kinetic energies well below 0.3 K.

The rotating beam source considered here is an exploratory prototype,[5] of limited capabilities, but already adequate for a variety of applications. We describe the construction of the rotating source, experiments and analysis assessing its performance, and prospective improvements. The apparatus required is relatively simple, compact, and versatile. Although our current focus is on slowing molecules, the speeding mode should find wide use. A rotating supersonic source can provide a fast pulsed beam with a much narrower velocity spread than the swatting technique, which relies on thermal evaporation from the rotor tip.

Contrariwise, in pursuing the slowing mode, we were led (by limited pumping capacity) to examine a multichannel effusive source, which has a broad velocity distribution. We find the low-velocity tail of the rotating effusive beam (absent in the supersonic case) has an unexpected virtue; model calculations indicate conditions under which the tail may provide a useful means to load a molecular trap.

Aspects of a Rotating Molecular Beam

Figure 1 shows the basic scheme. Gas is fed into a hollow rotor along its axis and exits from an aperture near the tip of the rotor arm. The flow velocity of the emergent molecular beam in the laboratory frame, **V**, is a vector sum of the flow velocity in the rotor's reference frame, **X**, and the peripheral velocity of the rotor, $\boldsymbol{V}_{\mathrm{rot.}}$. Depending on the direction of rotation, the resultant $\boldsymbol{V}_{\mathrm{rot.}}$ can augment **X** (speeding mode) or cancel much of **X** (slowing mode, as pictured) or even override **X** ("super-slowing" mode, in which **V** points opposite to **X**), thereby accelerating or decelerating the molecular beam. Four basic aspects (other than engineering issues) affect the performance of such a rotating molecular beam source: the transformation of flux from a rotating to laboratory-fixed frame; centrifugal enhancement of gas density within the rotor; swatting of molecules too slow to escape the path of the rotor; and the markedly velocity-dependent attentuation of the beam by collisions with background gas.

Gas Kinetic Analysis. The distribution of molecular flux, $F(X)\ \mathrm{d}X$, emitted from the rotor with Cartesian velocity components in the range $X_x \rightarrow X_x + \mathrm{d}X_x$, $X_y \rightarrow X_y + \mathrm{d}X_y$, $X_z \rightarrow$

† Part of the special issue "Harold Johnston Festschrift".

‡ Present address: Department of Chemistry, Stanford University, Stanford, CA 94305.

10.1021/jp002640u CCC: $20.00
Published on Web 01/03/2001

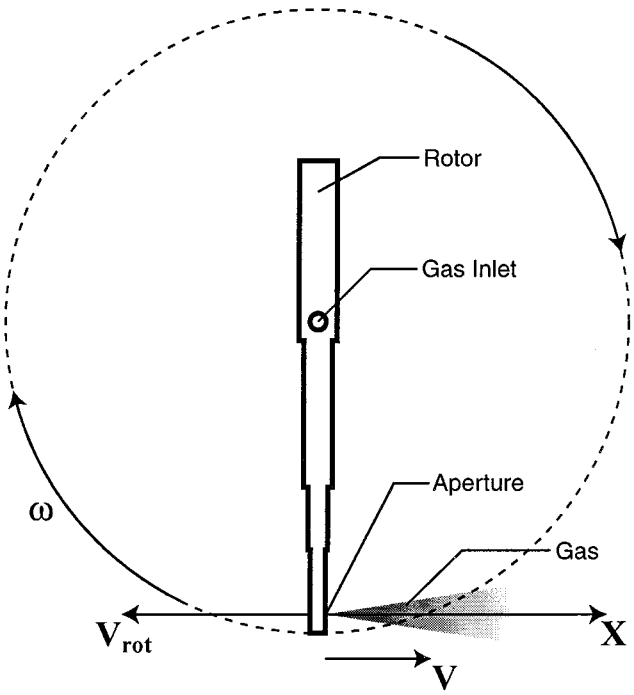

Figure 1. Schematic (top view) of rotating source, in slowing mode. Gas is fed into a hollow rotor, spinning about the inlet at an angular velocity ω, and emerges as a molecular beam (shaded cone). Peripheral velocity of the rotor, $V_{rot.}$, partially offsets flow velocity of molecular beam, X, resulting in a smaller laboratory velocity, **V**. In the case in which $V_{rot.}$ exceeds **X** in magnitude, **V** points opposite to **X**; this is referred to as the "superslowing" mode. If sense of rotation is reversed, so that $V_{rot.}$ and **X** are in the same direction, source operates in a speeding mode.

$X_z + dX_z$ has the approximate form

$$F(X)\,dX = CX\exp\{-[(X-u)/\Delta v]^2\}dX_x\,dX_y\,dX_z \quad (1)$$

For a supersonic beam, u denotes the flow velocity along the centerline of the beam, Δv represents the velocity spread (full width at half-maximum (fwhm $\approx 1.65\Delta v$), and C specifies the total flux intensity.[13] These quantities can be evaluated from standard approximate formulas for supersonic expansions,[13−16] involving the molecular mass, m; heat capacity ratio, $\gamma = C_p/C_v$; collision cross-sections; gas temperature T_o and pressure P_o within the source; and nozzle diameter, d. The flow velocity and spread are given by

$$u = \alpha_o[\gamma/(\gamma-1)]^{1/2}[1-(T_{||}/T_o)]^{1/2} \quad (2)$$

$$\Delta v = \alpha_o(T_{||}/T_o)^{1/2} \quad \text{with} \quad \alpha_o \equiv (2k_BT_o/m)^{1/2} \quad (3)$$

where α_o is the most probable velocity within the source and k_B is Boltzmann's constant. The parallel temperature, $T_{||}$, describes the molecular translational motion relative to the flow velocity. According to the thermal conduction model,[14] $T_{||}/T_o$ is proportional to $(P_od)^{-\beta}$ with $\beta = 6(\gamma-1)/(\gamma+2)$, so the velocity spread becomes very small for a strong supersonic expansion. For an effusive beam, $u = 0$ and $\Delta v = \alpha_o$.

To transform the flux into the laboratory frame and find the flux distribution, $F(V)\,dV$, of molecules with a laboratory velocity between $V \rightarrow V + dV$, we replace the volume element in the rotor's frame, $dX_x\,dX_y\,dX_z$, with its appropriate laboratory equivalent, given by[3]

$$dX_x\,dX_y\,dX_z = \Omega V^2\,dV \quad (4)$$

where Ω is the solid angle subtended downstream by a skimmer or other defining slit. From Figure 1, $X = V - V_{rot.}$ with $V_{rot.}$ negative for the slowing mode and positive for the speeding mode. The flux thus becomes

$$F(V)\,dV = CV^2(V-V_{rot.})\exp\{-[(V-u_{lab})/\Delta v]^2\}\,dV \quad (5)$$

where $u_{lab} \equiv u + V_{rot.}$ is the effective flow velocity of the beam, in the laboratory frame. Since only molecules with $X > 0$ can be emitted from the rotor, $V > V_{rot.}$ in the speeding mode, whereas $V \rightarrow 0$ is accessible in the slowing modes.

A key aspect is the role of the V^2 factor in eq 5, which enters as a Jacobian in the volume element of eq 4. For a rotating source, this factor distorts the laboratory velocity distribution from what would result if the distribution emerging from the rotor were merely shifted up or down by $V_{rot.}$. As illustrated in Figure 2, the effect becomes very pronounced as $V \rightarrow 0$, and markedly reduces the flux of very slow molecules that can be obtained. This Jacobian constraint is simply a geometrical consequence of the spreading due to transverse velocity components (X_x, X_y), which becomes more and more important as the laboratory velocity is decreased.

In analysis of experiments and applications, three other distributions related to $F(V)$ are involved: those for flight time, t; laboratory translational kinetic energy, E; and deBroglie wavelenth, λ. Also, if the detector measures number density rather than flux, as is often the case, the density distribution $D(V) \equiv F(V)/V$ is required. When transformed to the time domain, this becomes $D(t) = D[V(t)](dV/dt)$. Since $t = L/V$, with L being the flight distance from the exit aperture of the source to the detector,

$$D(t) = (C/t)(L/t)^2(L/t - V_{rot.})\exp\{-[(L/t-u_{lab})/\Delta v]^2\} \quad (6)$$

The corresponding distributions for energy and wavelength may be obtained in analogous fashion; e.g., $F(E) = F[V(E)](dV/dE)$.

The scale factor C can be determined by relating it to the centerline intensity $I(0)$ when the rotor is stationary, as given by familiar formulas for either supersonic[13−15] or effusive[17] molecular beams. Integrating eq 5 (with $V_{rot.} = 0$, $u_{lab} = u$) over all velocities gives the total flux, $F_{tot.}$, in molecules s^{-1} cm^{-2}. Multiplying $F_{tot.}$ by the area of a defining slit (or skimmer) downstream, σ_s, and dividing by the solid angle subtended by the slit, Ω, gives the centerline intensity, $I(0)$, in molecules s^{-1} sr^{-1}, from which C can be evaluated numerically. With the source rotating at ω revolutions per second, the number of molecules in the pulse emitted into Ω for each rotor cycle, N_P, can then be determined from

$$N_P = \tau\sigma_s\int F(V)\,dV \quad (7)$$

where $\tau = (\Delta\theta/2\pi)(1/\omega)$ is the pulse duration (time the rotor spends aligned with the slit, defined by its angular width $\Delta\theta$ in the plane of the rotor orbit). The flux distribution pertains to the rotating source, and the velocity integration extends from 0 to ∞ for the slowing mode and from $V_{rot.}$ to ∞ for the speeding mode. The net intensity in molecules s^{-1} delivered to the skimmer is $I = \omega N_P$.

Centrifugal Effect. When the rotor is spinning, the gas molecules within are subjected to a centrifugal force directed outward and acquire a potential energy given by $-m\omega^2R^2/2$, where R is the distance along the rotor arm measured from the axis of rotation. This produces a density gradient within the rotor, increasing between the gas inlet on the rotation axis and the exit aperature at R_{out}. If the gas remains essentially at thermal

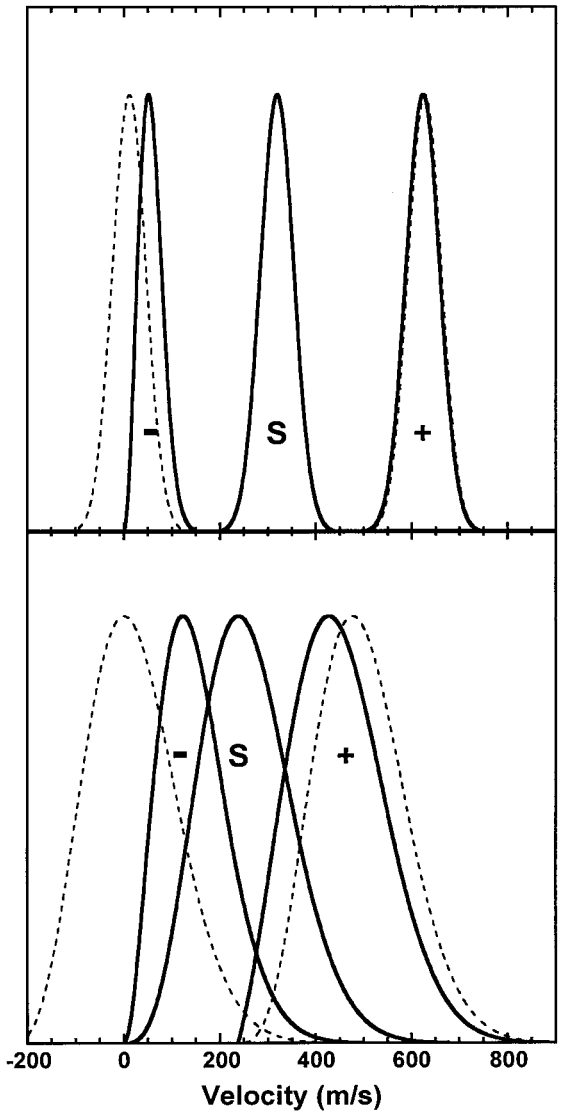

Figure 2. Velocity distributions calculated for supersonic beams (upper panel) and effusive beams (lower panel) of Xe, exhibiting effect of the V^2 Jacobian factor in eq 5 on the shape of the distributions. Full curves show velocity distributions for stationary beams (labeled S) and for beams from rotating source in the speeding mode ($V_{rot.} > 0$, labeled +) or slowing mode ($V_{rot.} < 0$, labeled −). Dashed curves show distributions that would be obtained if the stationary distribution were merely shifted up or down by the rotor. For the supersonic case, the flow velocity is $u = 308$ m/s and $V_{rot.} = \pm u$; for the effusive case, $u = 0$, the most probable velocity in the flux distribution is $(3/2)^{1/2}\alpha_o = 238$ m/s and $V_{rot.} = \pm(3/2)^{1/2}\alpha_o$.

equilibrium, the pressure behind the exit aperature, P_o, is governed by a Boltzmann factor,[18]

$$P_o = P_{in} \exp[mV_{rot.}^2/(2k_BT_0)] \quad (8)$$

with $V_{rot.} = 2\pi\omega R_{out}$. As illustrated in Figure 3, this centrifugal factor can make P_o much larger than P_{in}, particularly for heavy molecules and high rotational speeds. According to eq 3, this increase in the backing pressure can substantially lower $T_{||}$ and hence narrow the velocity spread. Since the beam intensity scales linearly with P_o, it is also enhanced by the centrifugal effect and thus increases exponentially with $V_{rot.}$ whenever eq 8 holds.[19]

On heuristic grounds, we expect that eq 8 should be a fair approximation as long as P_oA_{out} is substantially less than $P_{in}A_{in}$, where the A's denote areas of the exit and inlet apertures. In

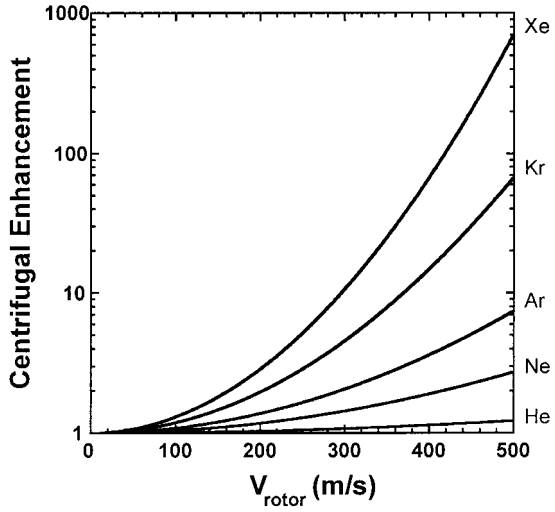

Figure 3. Centrifugal enhancement of gas density at the tip of the rotor as function of its peripheral velocity, according to eq 8: shown for He, Ne, Ar, Kr, Xe at a radius $R_{out} = 9.9$ cm from the gas inlet at the center of rotation.

our experiments using a supersonic beam source, $A_{out}/A_{in} < 100$. Therefore, we expect that for a wide range of P_o/P_{in}, gas within the rotor will remain close to equilibrium and eq 6 will apply. In other experiments using a multichannel effusive source, $A_{out}/A_{in} > 4$, and then we expect no appreciable centrifugal enhancement of the pressure.

Swatting Limit. Another consideration specific to a rotating source pertains to molecules emerging so slowly that they cannot escape being swatted by the rotor arm as it comes back around. As pictured in Figure 1, the exit aperture at R_{out} is not quite at the tip of the rotor arm, of length R_a. The molecules thus must travel a distance $(R_a^2 - R_{out}^2)^{1/2}$ to get beyond the orbit of the returning tip. This distance must be traveled in the time it takes for the rotor to turn through $(2\pi - \theta)$ radians, with $\cos\theta = R_{out}/R_a$. The minimum velocity, V_{min}, required to allow a molecule to escape swatting is therefore given by

$$V_{min} = V_{rot.}[(R_a/R_{out})^2 - 1]^{1/2}/(2\pi - \theta) \quad (9)$$

Our rotor has $R_a = 10.2$ cm and $R_{out} = 9.9$ cm, so its swatting limit is $V_{min} = 0.038V_{rot.}$. For example, if $V_{rot.} = 315$ m/s, the speed required to fully cancel the flow velocity of a supersonic beam of xenon, $V_{min} = 12$ m/s. The corresponding minimum translational kinetic energy for O_2 or CH_3F seeded in Xe is about 0.3 K, comparable to that attained by buffer gas cooling.[11]

Moreover, the swatting limit can be mitigated in several ways. These include placing the exit aperture closer to the rotor tip, shaping the tip to decrease the swatted area, or aiming the nozzle at a slight angle to allow molecules to escape above or below the plane of the rotor orbit.[20]

Attenuation by Scattering. Collisions with background gas weaken the beam intensity and are especially detrimental for slow molecules, which spend more time traversing the scattering region and have larger collision cross-sections. For a beam of molecules traveling a distance l at velocity V, the fraction still in the original beam is[21]

$$\varphi = \exp(-\Theta l/V) \quad (10)$$

with Θ the rate at which beam molecules collide with the

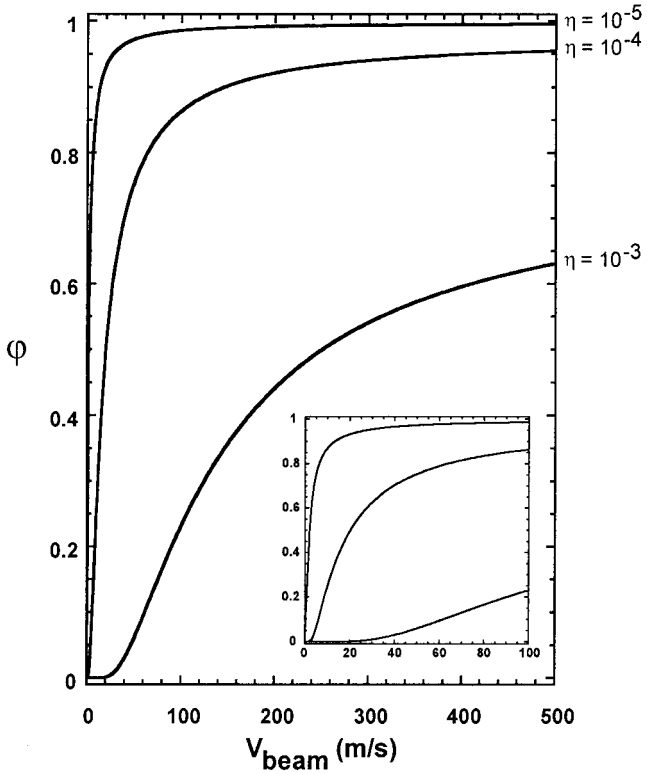

Figure 4. Attenuation of a molecular beam of Xe by scattering from the background gas as function of the beam velocity, according to eq 10: shown for Xe beam scattered by Xe, with $C_6 = 2.58 \times 10^{-65}$ J cm^6. Ordinate φ denotes the fraction of the original beam remaining after traveling a distance l through background gas at pressure P_b; parameter $\eta \equiv P_b l$ (in units of Torr·cm).

background gas, given by

$$\Theta = (nS\alpha_0/\pi^{1/2})[\exp(-x^2) + (2x + 1/x)\int_0^x \exp(-y^2)\,dy] \quad (11)$$

where n is the density of the gas, S the collision cross-section, and $x \equiv V/\alpha$, with α the most probable velocity of the gas. For slow molecules, the cross-section can be approximated as[22]

$$S = 2\pi\rho[C_6/(hV_{rel})]^{2/5} \quad (12)$$

where C_6 is the van der Waals interaction constant, h is Planck's constant, and V_{rel} is the relative velocity between beam and gas molecules. The factor ρ, less than unity, serves to correct for the imperfect angular resolution involved in scattering from a broad beam. We found $\rho \approx 0.6$ by measuring the attenuation of a Xe beam as a function of velocity and the background gas pressure. This factor, together with theoretical C_6 constants,[23] was used in evaluating the effective cross-sections for calculations of the expected attentuation by background gas.

Figure 4 illustrates such calculations for beams of Xe scattered by Xe. The fraction of surviving beam atoms, φ, is shown as a function of V and a parameter, $\eta \equiv P_b l$, involving the pressure of the background gas and the scattering path length. Under typical conditions in our experiments ($P_b \approx 10^{-4}$ Torr and $l \approx$ 10 cm) we have $\eta \approx 10^{-3}$ in the source chamber. Accordingly, the attenuation calculations indicate drastic scattering of slow molecules: for $V < 70$ m/s more than 90% and for $V < 20$ m/s more than 99% of the molecules are lost from the beam. Since the pressure dependence is strongly exponential, however, much of this attrition can be avoided by better pumping. If P_b were lowered 10-fold, the loss via scattering of molecules with $V <$ 20 m/s would be about 50%.

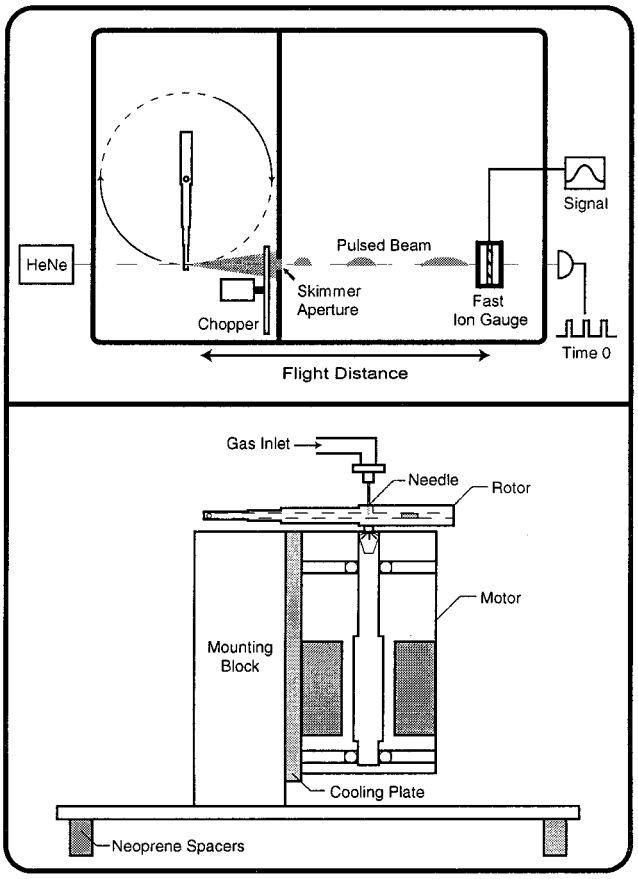

Figure 5. Experimental apparatus. Upper panel shows (top view) setup for time-of-flight velocity analysis. Rotating molecular beam source interrupts light from a HeNe laser to provide time zero. Pulses of molecules passing through skimmer aperture are detected by fast ion gauge (or quadrupole mass spectrometer). Chopper wheel modulates beam to enable time-of-flight measurements when rotor is stationary or beam pulses overlap. Lower panel shows (plan view) details of rotor, gas feed, and drive mechanism, including components to provide water-cooling and to damp vibrations.

Experimental Apparatus and Procedures

Figure 5 shows essential features of our apparatus. A thorough description including design calculations is given elsewhere.[16] The vacuum envelope is divided into source and detector chambers which communicate only by a circular hole (0.64 cm diameter) that serves as a beam skimmer. The source chamber is pumped by 10 and 6 in. diffusion pumps; the detector chamber, by a 6 in. diffusion pump with a baffle cooled by liquid nitrogen. Without a molecular beam, the background pressure is about 10^{-6} Torr in the source chamber and typically more than 3-fold lower in the detector chamber. When gas at up to 100 Torr is fed into the rotor, the pressure in the source chamber rises to about 10^{-4} Torr.

As the rotor spins, the molecular beam (shaded cone) emerging from the exit aperature near the rotor tip sweeps briefly over the skimmer hole, located $L_1 = 10.5$ cm downstream. This sends a pulse of molecules into the detector chamber on each rotor cycle. The central portion of the pulse passes through a second collimating hole (0.32 cm diameter) located $L_2 = 13.5$ cm beyond the skimmer.[24] Transmitted molecules are detected by either a fast ion gauge[25] or a quadrupole mass spectrometer[26] backed by a channeltron. The distance to the ionization zone was variable from 20 to 86 cm beyond the second collimator.

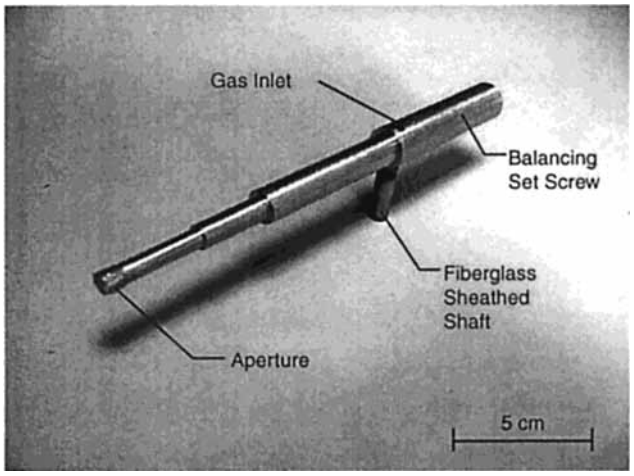

Figure 6. Rotor (final version; details in text). The exit aperture contains either a pinhole nozzle to produce a supersonic beam or a glass capillary array to provide a multichannel effusive source.

The rotor position is monitored by a HeNe laser beam and a photodiode to provide a time zero for measurements of time-of-flight (TOF) distributions. A chopper wheel (10.2 cm diameter, with two slots 0.32 cm wide) in the source chamber serves to modulate the molecular beam and thereby enable TOF measurements when the rotor is stationary. The chopper is also used to remodulate the beam when the rotor is spinning very rapidly and the molecular pulses are traveling so slowly that adjacent pulses overlap.

The rotor is mounted on a stainless steel shaft which is grasped by a collet connected to a spindle driven by a vacuum-adapted high-speed motor. It is an AC induction motor[27] operated by a three-phase digital power source and equipped with high-precision ceramic bearings (silicon nitride) that are lubricated with a nonvolatile vacuum grease.[28] The motor is bolted to a water-cooled copper plate[29] held at approximately 18 °C. This plate in turn is bolted to a 7.7 kg stainless steel block to damp internal vibrations of the motor. The block is attached to an aluminum breadboard (3/8 in. thick) connected to the vacuum chamber by four neoprene spacers (3/4 in. tall) which further damp vibrations. In operation, the motor was driven up to 700 rps (42 000 rpm), corresponding to a peripheral velocity of 434 m/s for the rotating source.

It proved challenging to develop a hollow rotor capable of providing peripheral velocities in the molecular range. In initial attempts we tried several versions of tubular rotors, of symmetrical double-bladed form with endcaps soldered on each end. All promptly lost endcaps or broke apart or wobbled pitifully when spun at high speeds. We finally arrived at a single-bladed design which required no endcaps. This rotor, shown in Figure 6, is easy to fabricate and has proved quite durable, operating without mishap for a year in about 200 runs. The hollow bore of the rotor (0.125 in. diameter) extends almost to its tip (within 0.030 in.). At the short end the bore is threaded and sealed by a 8−32 set screw (0.375 in. long, 0.146 in. diameter). This screw also enables precise static balancing of the rotor, which was found to be sufficient to ensure smooth, wobble-free spinning even at high speeds. The rotor barrel (mass 29 g) is made of an aluminum alloy (7075-T6); its ratio of tensile strength to density (1.8×10^5 m^2 s^{-2}) is nearly as high as that for titanium. The taper of the rotor was done in four steps, to facilitate machining. From thick to thin, the diameters of the four cylindical segments are as follows: 0.500, 0.374, 0.262, and 0.200 in. Their lengths are as follows: 2.150, 1.940, 0.831, and 1.099 in., respectively. These dimensions, as determined from computations analyzing the centrifugal forces for various rotor shapes,[16] maximize the peripheral velocity at which the rotor should break; this theoretical limit is 615 m/s.

The rotor shaft (0.200 in. diameter) is press fit into the underside of the barrel, with the center of the shaft 4.000 in. from the rotor tip and 2.019 in. from the thick end. A sheath of G-10 fiberglass (0.025 in. thick) about the shaft minimizes heat conduction from the motor to the rotor. The gas inlet, on the topside of the rotor barrel, receives gas fed in via a greased stationary needle that is slightly smaller (0.0625 in. diameter) than the hole in the barrel. In early runs, we used needles of Teflon or tefzel, but found that at high rotor speeds these often rapidly eroded. Much better performance was attained using a needle (0.025 in. i.d.) of PEEK[30] (polyetheretherketone); it has flexibility and low friction similar to Teflon, but is more robust. PEEK needles have withstood rotor speeds up to 650 rps in prolonged runs with little or no scuffing or deformation.

To provide the exit aperture of the rotor, flat regions were machined on both sides and a tangential hole (0.060 in. diameter) drilled near the tip. This hole was covered by shingle patches attached by epoxy. One patch bears the gas exit. For runs with supersonic beams, this was a stainless steel disk (0.0005 in. thick, 0.118 in. diameter), with a laser-drilled pinhole nozzle (100 μm diameter). For runs with effusive beams, the disk was replaced with a compact glass capillary array[31] (pore diameter, 10 μm; length, 500 μm; 50% transparency). The patch on the side opposite the gas exit was a Lexan sheet ($0.010 \times 0.125 \times$ 0.200 in.) that transmits the monitor beam from the HeNe laser.

Procedures for apparatus alignment and time-of-flight measurements were straightforward. Since the detectors used respond to number density, the basic observable quantity is the $D(t)$ function of eq 6. If the molecules were emitted only when the rotor reached its nominal "shooting" position, the TOF data could be directly fit to $D(t)$ to evaluate u_{lab} and Δv for a supersonic beam or α_0 for an effusive beam. However, the skimmer and collimating slit configuration allows the rotor to emit detectable molecules within $\pm 8°$ of the nominal shooting position. The TOF data thus must be deconvoluted with a shutter function of approximately square-wave form,[16] using standard methods.[32] To keep the effect of deconvolution small (typically $\sim$10% for u_{lab} and Δv), we increased the flight distance to the detector (as indicated in Figure 5) for measurements made at low rotor speeds ($V_{rot.} < 100$ m/s). As long as the overlap of adjacent molecular pulses remained modest, we found good results for u_{lab} and Δv or α_0 could be extracted by fitting the entire pulse train. When the overlap became pronounced, usually for $V \leq 100$ m/s, the chopper was used, as noted above, to enable TOF measurements. The chopper was typically operated at 300 rps, which provided a shutter width of only 100 μs, allowing good resolution. Use of the chopper markedly reduced the detectable beam intensity, however, as the duty cycle was 5%. Although pulse overlap prevented measurement of very slow velocities down to the swatting limit, in practice the loss of intensity due to the V^2 Jacobian factor and to attenuation by collisions proved more serious, seldom allowing useful data to be obtained for $V < 50$ m/s.

Results and Analysis

To compare the performance of the rotor source with theory, we obtained extensive TOF and beam intensity data for a wide range of source conditions, with the rotor stationary as well as run in the slowing and speeding modes. We first describe results obtained in the supersonic regime for pure beams of Ne, Ar, Kr, Xe, O_2, CH_3F, and SF_6 and seeded beams of O_2 and CH_3F in Xe. Table 1 lists parameters for representative runs.

TABLE 1: Parameters for Rotating Supersonic Beams

species	P_0d, Torr·cm	$V_{rot.}$, m/s	u_{lab}, m/s	E_{lab}/k_B, K	λ_{lab}, Å	Δv, m/s	$T_{\|\|}$, K
Ne	0.542	−372	340	139	0.582	195	46
Ne	0.579	+403	1144	1574	0.173	174	36
Ar	1.12	−403	170	70	0.582	87	18
Ar	1.02	0	518	645	0.191	75	14
Ar	1.15	+403	974	2282	0.102	64	10
Kr	2.09	−341	42	8.9	1.12	17	1.5
Kr	0.8	0	364	669	0.130	50	12
Kr	4.56	+403	802	3249	0.059	23	2.6
Xe	1.03	−273	59	27	0.512	31	7.7
Xe	1.04	0	295	686	0.102	34	9.1
Xe	17.1	+403	720	4084	0.042	18	2.6
O_2	0.867	−403	281	152	0.440	176	59
O_2	0.32	0	588	665	0.210	205	81
O_2	0.873	+403	1084	2261	0.114	164	52
CH_3F	0.756	−403	304	189	0.383	193	76
CH_3F	0.387	0	664	902	0.175	195	78
CH_3F	0.894	+403	1120	2565	0.104	168	58
SF_6	2.31	−310	55	27	0.493	80	57
SF_6	0.224	0	307	828	0.088	94	77
SF_6	16.6	+403	763	5112	0.036	68	41
O_2 in Xe	1.53	0	299	172	0.414	39	2.9
O_2 in Xe	1.83	−248	67	8.6	1.85	85	14
CH_3F in Xe	1.52	0	319	208	0.365	43	3.7
CH_3F in Xe	1.66	−248	91	17	1.28	94	18

Stationary Supersonic Beams. With the rotor stationary, data were taken using the chopper with the fast ion gauge and sealing the gas input tube to the rotor inlet to eliminate leaking. The flow velocity u and Δv were determined for a 5-fold range of stagnation pressure within the source ($P_o = 20-100$ Torr). As expected, the results for Ar, Kr, and Xe beams ($\gamma = 5/3$) conform closely to eqs 2 and 3, with $T_{||}$ evaluated from the thermal conduction model.[14,16] For the beams of molecular gases, the agreement is likewise quite good, but only if vibrational contributions to the heat capacity ratio were omitted, so that the effective $\gamma = 7/5$ for O_2 and 8/6 for CH_3F and SF_6. For a stiff diatomic like O_2, vibrational energy is not expected to couple into the expansion, but this is less obvious for the polyatomic molecules, especially SF_6, which has many low-frequency modes. If heat capacity ratios given by thermal data[33] ($\gamma = 1.278$ and 1.094 for CH_3F and SF_6, respectively) are used, however, the usual formulas for u and especially Δv deviate widely from our experimental results.

For Ar, Kr, and Xe beams we also examined the variation of intensity with P_o, which in our range should be linear according to the standard theory.[13−15] At low source pressures our results conform well, but droop increasingly below the predicted lines as P_o is increased; the deviations set in near 30, 40, and 50 Torr respectively for Ar, Kr, and Xe. Attenuation by collisions with background gas, as given by eq 10, was found to largely account for these deviations. Experimental estimates of the intensity of these beams of the order of 10^{18} molecules s^{-1} sr^{-1} for $P_o = 30$ Torr and $d = 0.01$ cm, were also derived from geometrical factors and the ion gauge sensitivity, again in fair agreement with the theory of supersonic expansions.

Seeded supersonic beams of O_2 and CH_3F in Xe were examined using the mass spectrometer detector. The runs were made with a constant partial pressure of the seed molecule of about 5 Torr, and the pressure of Xe carrier gas was varied. Thereby the mole fraction of the seed molecule was scanned from about 0.4 to 0.1 as the total P_o ranged from 35 to 150 Torr. The experimental values of u and Δv for the seed molecules agree fairly well with calculations[16] employing a theory of seeded beams presented by Miller,[15] almost within the range of experimental error and uncertainties in requisite parameters. According to the theory, $T_{||}$ should be lower for the seed species than the carrier gas, a distinctive feature of "inverse" seeding (light seed, heavy carrier). We found this holds for values of $T_{||}$ derived from our Δv results. However, whereas the theory predicts that the seed molecule should have a flow velocity near to but higher than that of the Xe carrier gas, we found u_s is consistently lower than u_c by 5−10%. Although seeding of a light molecule in a heavy carrier gas indeed makes u_s and Δv_s much lower than for a pure beam of the seed molecule at the same P_o, the centerline intensity of the seed species is reduced both by its small mole fraction and by a further factor of about m_s/m_c due to mass defocusing. These effects together typically lower the intensity by roughly a 100-fold.

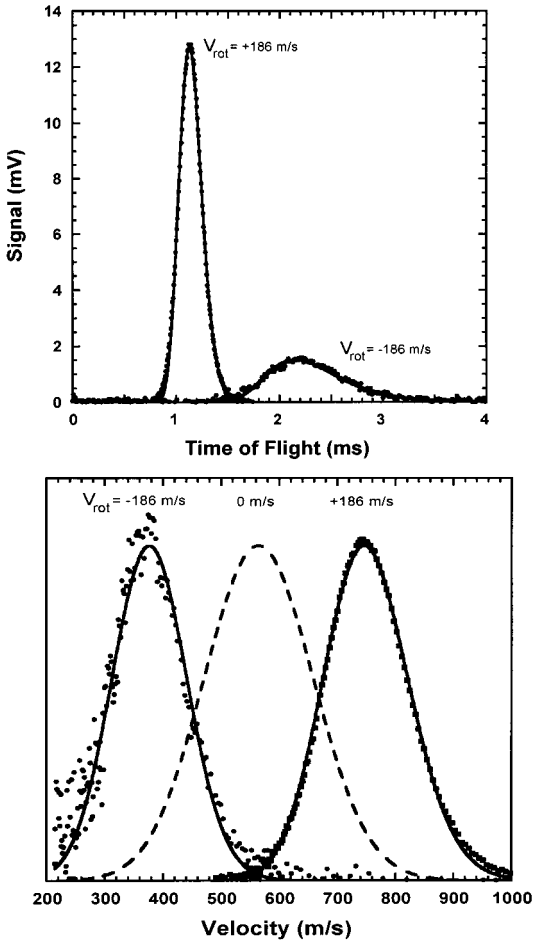

Figure 7. Sample data. Upper panel shows measured time-of-flight distributions (points, taken with $L = 86$ cm flight path) for a supersonic beam of argon ($P_{in}d = 0.3$ Torr cm, $T_o \approx 300$ K, $u \approx 550$ m/s) from rotor operated in the speeding ($V_{rot.} = 186$ m/s) or slowing mode ($V_{rot.} = -186$ m/s). Curves show fit of $D(t)$ distribution of eq 6 (with $u_{lab} = u \pm V_{rot.}$, $\Delta v = 103$ m/s). Lower panel shows same data and curves transformed to velocity flux distributions, $F(V)$ of eq 5 (but normalized to the same peak height). Dashed curve depicts $F(V)$ for a stationary beam.

Rotating Supersonic Beams. Figure 7 shows typical TOF data for an Ar beam from the rotating source, obtained for both the slowing and speeding modes, together with the fitted $D(t)$ and $F(V)$ distributions. As expected, the distributions are shifted by approximately $\pm V_{rot.}$ and are slightly narrower than that for a stationary beam. The narrowing is attributable to a decrease in $T_{||}$ produced by centrifugal enhancement of the backing pressure. The large difference in peak heights for the slow and fast TOF distributions is due to the t^{-2} Jacobian factor in eq 6; this factor also amplifies the noise at long times (slow speeds).

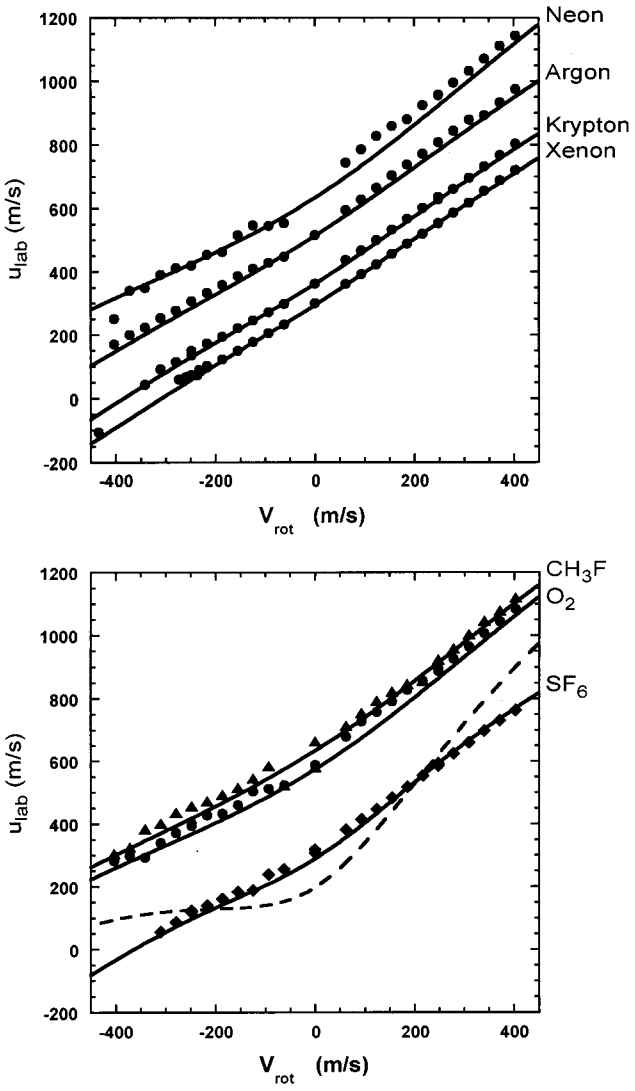

Figure 8. Variation of u_{lab}, laboratory flow velocity fitted to eq 5, with $V_{rot.}$, peripheral velocity of source due to rotor. Negative $V_{rot.}$ corresponds to operation in the "slowing mode," positive to the "speeding" mode; negative u_{lab} corresponds to "backwards slowing" mode (cf. Figures 1 and 11). Curves are computed as described in the text; nonlinearity is due to the centrifugal contribution. Upper panel displays the experimental results (points) and prediction (curves) for the rare gas atoms. Lower panel shows similar results for O_2 (●), CH_3F (▲). and SF_6 (◆). Dashed curve shows predicted behavior for SF_6 with $\gamma = 1.1$.

The higher density of data points for the speeding mode results from the higher sampling rate for short times.

Figure 8 displays the effective flow velocity, $u_{lab} = u + V_{rot.}$, as obtained from fitting TOF data for both the slowing and speeding modes. The full curves show results predicted with the flow velocity u computed from eq 2, including the contribution of centrifugal enhancement to $T_{||}$, which accounts for the modest deviation from linearity. The experimental and predicted results agree well and illustrate the wide range of velocities made accessible by the rotating source.

As seen in eq 8, the centrifugal enhancement of the backing pressure depends on $V_{rot.}^2$, so is independent of the direction of rotation. Figure 9 illustrates the marked drop in $T_{||}$ due to the centrifugal effect and its similarity for the slowing and speeding modes. Since P_{inlet} was held constant, if there were no centrifugal enhancement, $T_{||}$ would be unaffected by the rotor speed. Unlike u_{lab}, values obtained for Δv and therefore for $T_{||}$ are rather sensitive to measurement and fitting errors, as well as theoretical

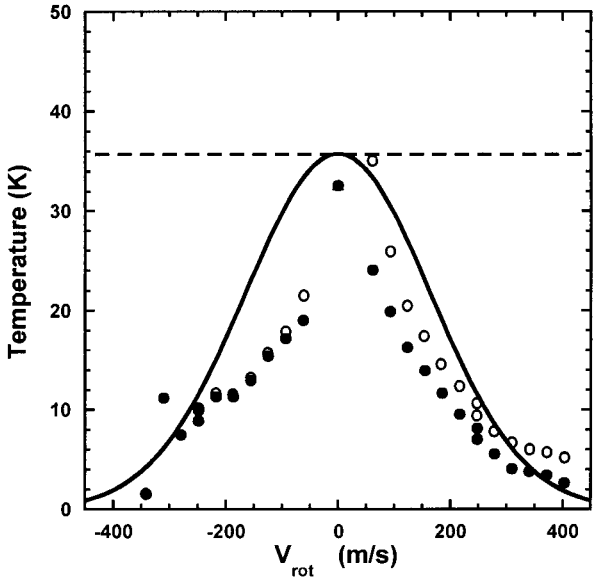

Figure 9. Centrifugal effect for supersonic Kr beam ($P_{inlet}d = 0.3$ Torr·cm) as a function of $V_{rot.}$. Points show values of parallel temperature, $T_{||}$, derived from velocity spread via eq 3, with (●) and without (○) including the pulse width convolution. Full curve shows $T_{||}$ predicted by thermal conduction model[13,14] with source pressure P_o enhanced by centrifugal effect, as given by eq 8; dashed line shows result without centrifugal enhancement.

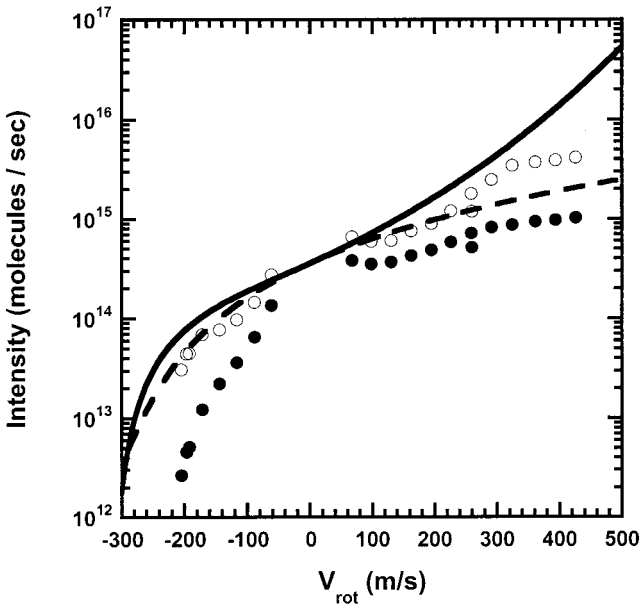

Figure 10. Variation of intensity with $V_{rot.}$ of a supersonic beam of Xe ($P_{inlet}d = 0.3$ Torr·cm) from rotating source. Upper abcissa scale shows corresponding values of $u_{lab} = u + V_{rot.}$. Full curve calculated from eqs 5 and 7, including centrifugal effect of eq 8; dashed curve omits centrifugal contribution. Points show experimental results (●) and data corrected (○) using eq 10 to estimate intensity expected in the absence of scattering by background gas.

approximations. We suspect the deviations between experimental and predicted values of $T_{||}$ arise largely from this sensitivity. Data confirming the centrifugal effect on $T_{||}$ over a 6-fold range of P_{inlet} with $V_{rot.}$ ranging from −62 m/s to −260 m/s are presented elsewhere.[5,16]

Figure 10 illustrates the strong variation of intensity with the rotor speed and direction even for runs with P_{inlet} held fixed. The full and dashed curves show the predicted variation of intensity respectively with and without the C factor in eq 1 scaled to include centrifugal enhancement. Note that the

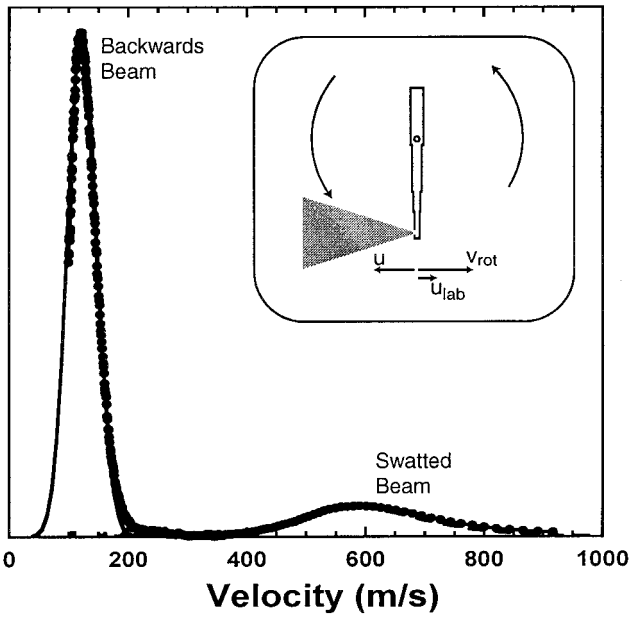

Figure 11. Velocity distribution of supersonic beam of Xe ($P_{inlet}d$ = 0.3 Torr·cm) emitted from rotor spinning more rapidly ($V_{rot.} = -434$ m/s) than the flow velocity ($u = 308$ m/s), in the opposite direction (see insert). Narrow peak at low velocities corresponds to beam traveling "backwards" with $u_{lab} \sim -107$ m/s; $\Delta v \sim 31$ m/s ($T_{\parallel} = 7.6$ K). Broader peak at higher velocities is from swatting of background gas with $u_{lab} \sim 543$ m/s and $\Delta v \sim 194$ m/s (~300 K).

divergence between the full and dashed curves for the speeding mode ($V_{rot.} > 0$) but not the slowing mode ($V_{rot.} < 0$) is not significant, but just reflects the different range in rotor speed. Full and open points show experimental intensity estimates respectively without and with correction for attentuation by scattering from background gas. The experimental points are inaccurate by at least a factor of 2, due to uncertainties in ion gauge efficiencies and collection volumes. Moreover, the correction for background scattering is large, because the gas inlet for the rotor is leaky and especially at high rotor speeds the centrifugal enhancement further increases the nozzle throughput and thus the background gas pressure. The experimental intensity, corrected for scattering, nonetheless agrees well with the theoretical model.

As compared with a stationary source operating with the same P_{inlet} and nozzle diameter, in Figure 10 the intensity drops 100-fold for slowing by $V_{rot.} = -200$ m/s (to $u_{lab} = 100$ m/s) and grows for speeding by about 10-fold for $V_{rot.} = 200$ m/s and by 100-fold for $V_{rot.} = 400$ m/s. This strong variation arises from the dependence of eqs 5 and 7 on $u_{lab} = u + V_{rot.}$ even when u, Δv, and C in eq 5 remain fixed (i.e., neglecting the centrifugal effect).

Our inability to measure very slow beams directly led us to seek to demonstrate that the rotor could produce a beam traveling "backward". As shown in Figure 11 (inset), in a "superslowing" mode, when $V_{rot.}$ becomes larger than u and is oppositely directed, the laboratory flow velocity will be reversed. In Figure 11, the data points show a velocity distribution obtained for a Xe beam with $V_{rot.} = -436$ m/s and $u = 310$ m/s, observed with the detector positioned on the backside of the nozzle. The distribution has two distinct peaks, a broad peak at high velocities (~600 m/s) and a narrow peak at lower velocities (~126 m/s). The high-velocity peak corresponds to background molecules swatted by the rotor[2-4] and the slower peak to molecules emitted from the nozzle, traveling backward. The high-velocity peak occurs near $\alpha_0 - V_{rot.}$ (with $\alpha_0 = 195$ m/s) and the slow peak near $u + V_{rot.}$, as expected. We confirmed the assignment by detaching the gas inlet from the rotor and raising the background pressure to a similar level ($P_b \sim 10^{-4}$ Torr). That caused the peak attributed to the backward beam to disappear, but the swatted peak remained.

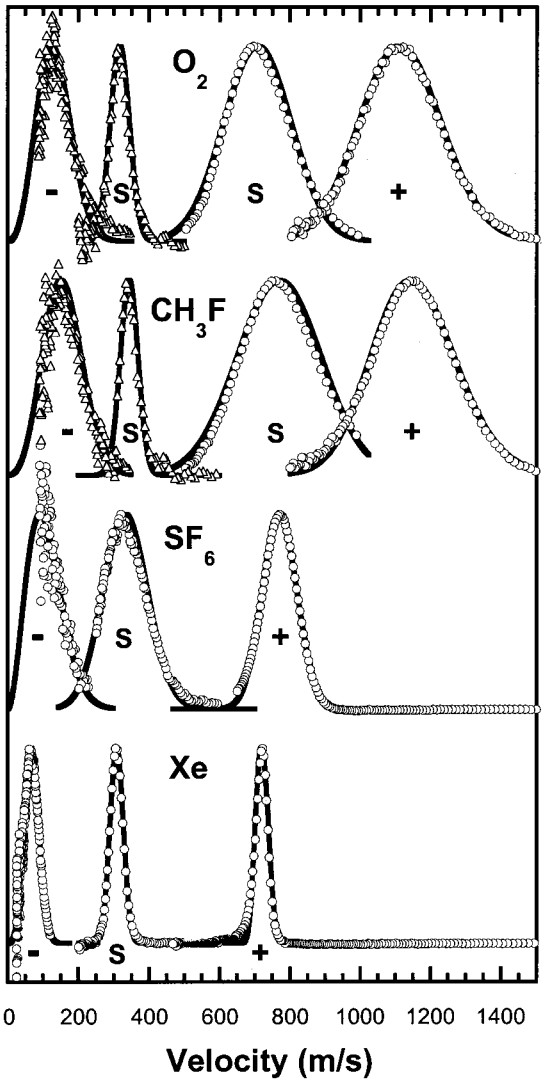

Figure 12. Velocity distributions for supersonic beams of Xe, SF_6, CH_3F, and O_2, with rotor stationary (S) or operated in speeding (+) or slowing (−) modes. Data points for pure beams are shown by circles (○) and for molecules seeded in Xe by triangles (△). Curves show fits to eq 5 with parameters given in Table 1.

Since the rotor speed feasible with our current apparatus ($|V_{rot.}| \leq 434$ m/s) is far below the flow velocity of supersonic beams of light molecules such as O_2 ($u \sim 740$ m/s) or CH_3F ($u \sim 765$ m/s), we tried inverse seeding in Xe ($u \sim 308$ m/s) as a means to obtain slow beams of the molecules. The procedure was the same as described above for stationary beams, except that the leaky inlet employed with the rotating source limited us to lower backing pressures ($P_{inlet} < 30$ Torr). Likewise, the cost in intensity of inverse seeding (roughly a factor of 100, from the combined effect of small seed ratio and mass defocusing) prevented use of the chopper to extend the velocity analysis below about 100 m/s.

Figure 12 compares velocity distributions obtained for supersonic O_2 and CH_3F beams, pure or seeded in Xe, with the source stationary or rotating. Inverse seeding is seen to markedly reduce both the flow velocity and velocity spread for the seed species. Surprisingly, however, when the source is rotated to

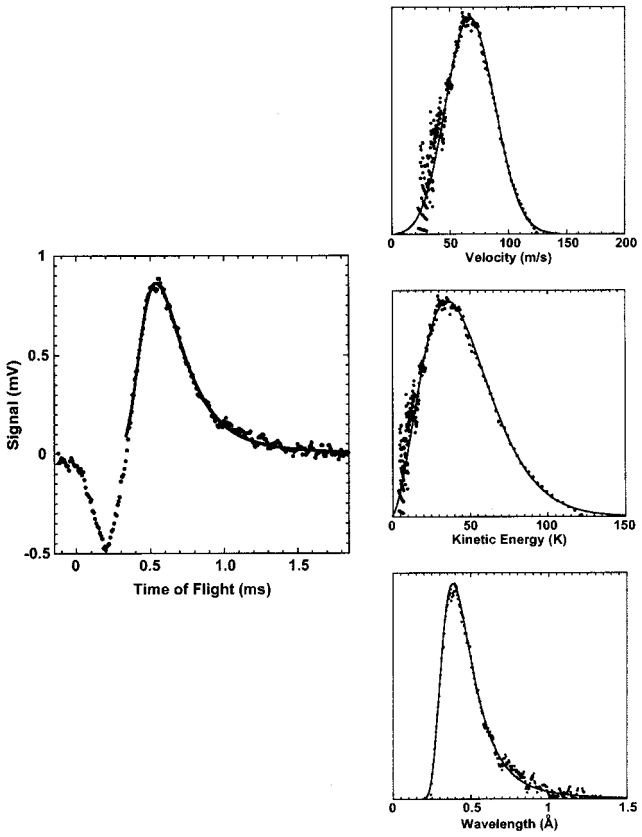

Figure 13. Slowest Xe beam obtained from rotating supersonic source ($P_{\text{inlet}}d$ = 0.15 Torr·cm) at $V_{\text{rot.}} = -273$ m/s. Panel at left shows experimental TOF distribution (for flight path of $L = 4.25$ cm) and fit to eq 6, which gives $u_{\text{lab}} = 59$ m/s and $\Delta v = 31$ m/s ($T_{\parallel} = 7.6$ K). Data were obtained using chopper to remodulate overlaping beam pulses. Initial dip at short times is due to modulation of background gas (confirmed in auxiliary runs); it is not included in the fit. Panels at right show same data transformed to flux distributions of velocity, translational kinetic energy, and deBroglie wavelength.

further slow the seeded beam, Δv becomes larger than for the stationary seeded beam. This is contrary to the narrowing anticipated from the centrifugal enhancement of the backing pressure and requires further study.[34] Figure 12 includes results for pure O_2 and CH_3F beams produced in the speeding mode. Altogether the range of most probable velocities in the slowed and speeded distributions shown span more than a factor of 10, and thus more than 100 in the corresponding translational kinetic energy.

Figure 12 also includes results for pure supersonic beams of Xe and SF_6. As seen in Table 1, for these systems as well as for pure Kr and for O_2 seeded in Xe, we were able to obtain laboratory flow velocities below 70 m/s by rotary slowing. As a summarizing paradigm, Figure 13 shows results for the slowest Xe beam we attained. The TOF data, which conforms very well to eq 6, is transformed as described thereunder to provide distributions of velocity, translational kinetic energy, and deBroglie wavelength. Table 1 includes corresponding parameters.

Rotating Effusive Beams. In the effusive regime, we studied beams of Xe, O_2, CH_3F, and SF_6. Several schemes designed to store molecules or manipulate their trajectories envision making use of the slow tail of a Maxwell−Boltzmann velocity distribution but are handicapped by its low intensity.[6,35−37] Rotating a multichannel source offers a means to produce slow effusive beams with substantial intensities.

In most runs made with the multichannel source, again with the ion gauge detector, we kept $P_{\text{inlet}} \leq 3$ Torr for all gases.

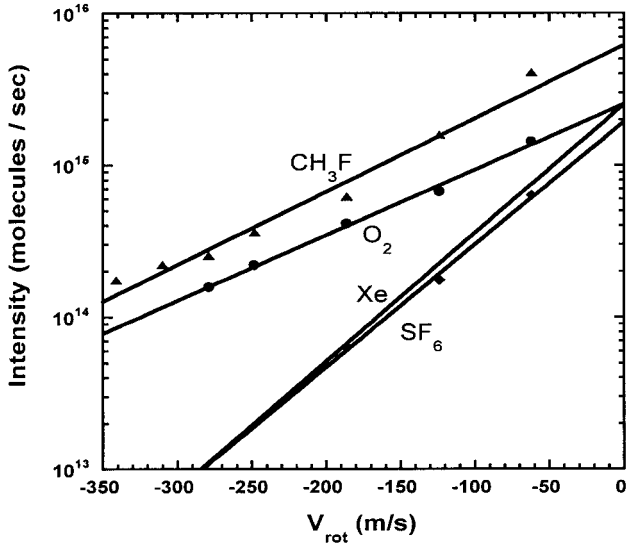

Figure 14. Variation of intensity with $V_{\text{rot.}}$ of effusive beams from rotating multichannel source of Xe (○), O_2 (●), CH_3F (▲), and SF_6 (◆). Runs made in slowing mode, with constant P_{inlet} (2 Torr for SF_6, 3 Torr for other gases). Curves calculated from eqs 5 and 7, normalized to experimental results for stationary beams.

This corresponds to what is termed the opaque mode,[17] in which the mean free path within the source exceeds the diameter of the channels but is considerably shorter than the channel length. As seen in eq 5, for a rotating effusive beam the velocity distribution is equivalent to that for a supersonic beam with $u_{\text{lab}} = V_{\text{rot.}}$ and $\Delta v = \alpha_o$. Measurements of TOF distributions over the range $V_{\text{rot.}} = 0$ to -350 m/s matched well that form. Values of α_0 fitted to the data were typically no more than 5% higher than those given by eq 3, even at high $V_{\text{rot.}}$, indicating any centrifugal effect is negligible. The angular distribution from the multichannel array was also measured and found to be only slightly wider (fwhm ≈ 10°) than expected for an ideal multichannel effusive source.[17]

Figure 14 shows how the intensity of the rotating effusive source varies with $V_{\text{rot.}}$. The observed intensity for a stationary beam was consistent with that calculated for a single-channel effusive beam, about 10^{14} molecules s^{-1} sr^{-1}, multiplied by an effective number of channels of the order of 30 000 or more, in rough accord with the number estimated from the area and transparency of the array.[31]

Figure 15, a counterpart to Figure 13, shows representative TOF data for a rapidly rotating effusive CH_3F beam. This illustrates how well overlapping adjacent beam pulses can be fitted by simple sums of terms of the form of eq 6, $D(t) + D(t + \tau) + ...$, although at low velocities the TOF overlapping eventually becomes too severe to provide useful data. The corresponding distributions of velocity, kinetic energy, and deBroglie wavelength (full curves) are compared with those for a stationary effusive beam (dashed curves). This exhibits the large enhancement of intensity at low kinetic energies and long deBroglie wavelengths produced by rotating the source.

Comparing Sources for Slow Molecules. In Figure 16, we assess the slow molecule output of the rotating supersonic and effusive sources in terms of translational kinetic energy, since that is a prime requisite for trapping or manipulating molecular trajectories. The full curves show intensities calculated from

$$I_{\text{slow}}(E^*) = G\int_0^{E^*} F(E)\,\mathrm{d}E = G\int_0^{V^*} F(V)\,\mathrm{d}V \qquad (13)$$

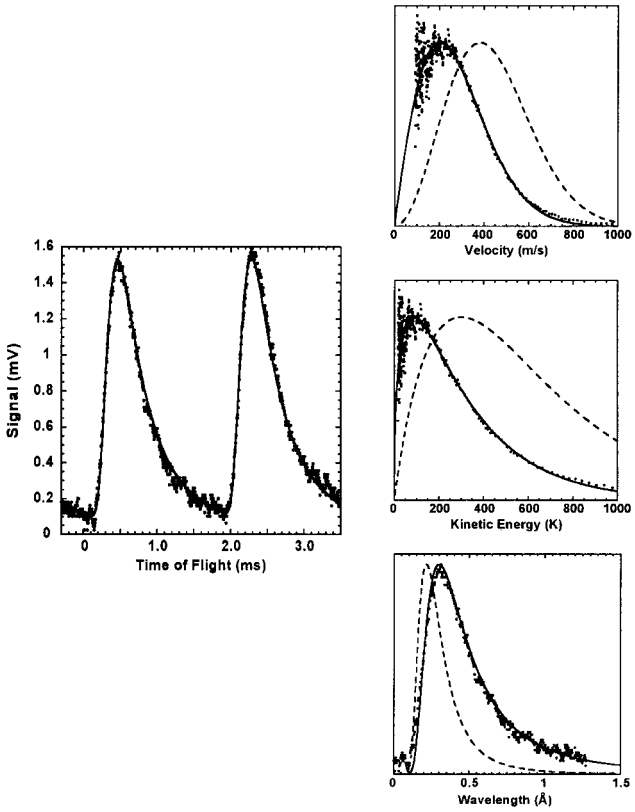

Figure 15. Slowest CH_3F beam obtained from rotating multichannel effusive source ($P_{inlet} = 3$ Torr) at $V_{rot.} = -341$ m/s. Panel at left shows experimental TOF distribution (for flight path of $L = 17.8$ cm) and fit to multiple beam pulses, which gives $\alpha = 401$ m/s, similar to $\alpha_o = 383$ m/s predicted for a Maxwellian beam at 300 K. Panels at right show same data transformed to flux distributions of velocity, translational kinetic energy, and deBroglie wavelength. Results for $V_{rot.} = 0$ are indicated by dashed curves.

where $G = \omega\tau\sigma_s$ is the geometrical factor from eq 7, and $V^* \equiv V(E^*)$. We consider slowing over a wide range of $V_{rot.}$ extending to kinetic energies lower than we could directly observe, but otherwise use parameters and conditions typical for CH_3F beams in our experiments.[38] The comparison is simple if attenuation by background gas and the swatting limit[20] are not taken into account. Then the pure supersonic beam (PS) strongly outdoes the inversely seeded supersonic beam (ISS), although not the multichannel effusive beam (MCE), when compared at the optimal $V_{rot.}$ for each. ISS has the advantage of a much lower $V_{rot.}$, but the small seeding fraction and mass defocusing drop its output of slow molecules 100-fold below MCE.

At $V_{rot.}$ speeds other than optimal, I_{slow} declines much more rapidly for PS and ISS than MCE. This reflects the narrow spread in kinetic energy of the supersonic beams in contrast to the much broader, thermal distribution and slow tail of an effusive beam. Another striking consequence stems from this difference. The optimal $V_{rot.}$ is close to the flow velocity for a supersonic beam, but it is considerably *lower* than α_o for an effusive beam. For MCE in Figure 16, the optimal $V_{rot.}$ is only $\sim$240 m/s, whereas $\alpha_o = 380$ m/s.

For our current apparatus, attenuation of slow molecules by background gas is a decisive factor. The higher source pressures for PS and ISS result in background 20-fold larger and attenuation of I_{slow} roughly 200-fold larger than for MCE. In the lower panel of Figure 16, dashed curves show the estimated effect of collisional attenuation. (For PS, it would actually be worse, due to the large increase in P_o from the centrifugal effect.) These calculations indicate that in practice the rotating effusive

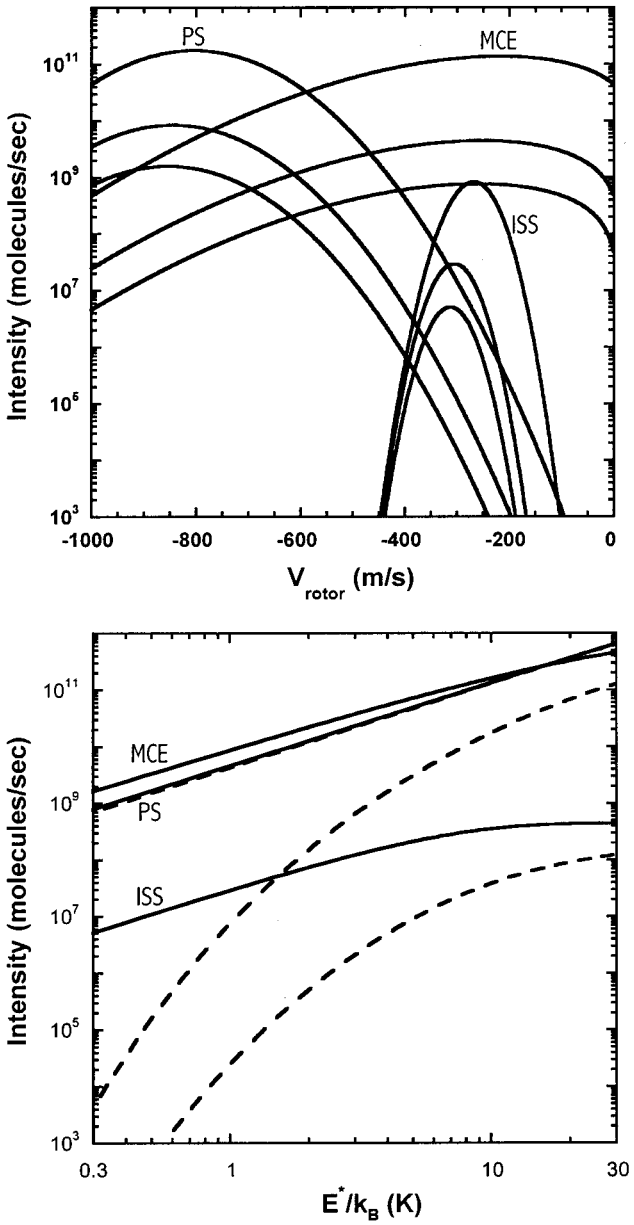

Figure 16. Comparison of molecular flux having translational kinetic energy below $E^*/k_B = 0.3$, 1, or 10 K for rotating supersonic and multichannel effusive beams of CH_3F in the slowing mode. Upper panel shows sets of curves for those three values of E^*, calculated from eq 13, for a pure supersonic beam (PS); for an inversely seeded beam in Xe carrier gas (ISS); and for a multichannel effusive beam (MCE). Lower panel plots variation with E^* of the maximum intensity attainable by optimal choice of $V_{rot.}$. Full curves in both panels computed without allowance for swatting limit[20] or attenuation by collisions; in the lower panel, dashed curves, respectively, include attenuation as calculated from eq 10, showing very large effect for supersonic beams and very little for the effusive case. Parameters were $G = 0.0035$, $T_o = 300$ K, $P_{inlet} = 30$ Torr for the supersonic beams (5% mole fraction in the inversely seeded case), 3 Torr for the effusive beam; $\eta = 10^{-3}$ Torr cm for supersonic cases, 10^{-5} Torr cm for effusive.

source can provide a substantially higher flux of molecules with low kinetic energies than either pure or seeded supersonic beams. This also compares very favorably with other slow molecule sources thus far implemented. Photoassociation within atom traps[39] provides the coldest molecules, but the yield is low and the chemical scope very limited. Deceleration by time-varying electric fields[12] is feasible for a sizable class of polar molecules and provides both state-selection and extremely narrow velocity spreads. Buffer gas cooling[11] is widely ap-

plicable, although it requires experiments to be performed within the cryogenic refrigerator, which can tolerate only a feeble heat load. Our mechanical method as yet does not provide very low kinetic energies, but it is widely applicable and requires relatively simple instrumentation.

Discussion

The current apparatus invites improvement in several respects. The background pressure in the source chamber can be reduced by stronger pumping and by redesign of the leaky gas inlet to include a differentially pumped antechamber. Also desirable but more difficult is a means to pulse the beam, synchronously with the rotor, to be emitted only in the "firing position". That would avoid the current 360° spray, which contributes most of the background. A possibility under study would use a laser pulse to open a heat-activated slit. Harvesting slow molecules could be much improved by directing the beam slightly below the rotor plane, to escape swatting,[20] and using a focusing field or storage ring configuration to offset the diluting effect of the V^2 Jacobian. Other means such as REMPI are available to measure slow velocities.[40] The range of the peripheral velocity, $V_{\text{rot.}}$, could be extended from the present 434 m/s to nearer the breaking limit of 615 m/s, either by improving cooling of our motor[29] or by increasing the length of the rotor. Much higher $V_{\text{rot.}}$, approaching 2 km/s, might be attained by using instead magnetic levitation and a carbon fiber rotor.[4]

In the mode used here, the rotating source can only generate beams of molecules with substantial vapor pressure. However, it may prove feasible to produce slow beams from nonvolatile substances, with requisite efficiency, by laser ablation[41] of samples from a rotor tip moving contrary to the velocity of the ejected molecules. Likewise, this technique could be applied to thermally fragile molecules by means of "matrix-assisted" laser desorption,[42] with the matrix and sample material supplied by auxiliary beams and condensed onto the rotor tip during its orbit.

In addition to its utility for many experiments facilitated by or requiring slow or fast molecules, the rotating source offers a means to readily scan velocity. As seen in Table 1, the current version of the rotating source can already alter the kinetic energy and the deBroglie wavelength of a molecule by sustantial factors, governed by $V_{\text{rot.}}/u$. Figure 17 provides a reduced variable plot illustrating, for both slowing and speeding modes, the accessible range in kinetic energy and deBroglie wavelength:

$$E_{\text{lab}}/E_{\text{u}} = (u_{\text{lab}}/u)^2 = (1 + x)^2 \tag{14}$$

$$\lambda_{\text{lab}}/\lambda_{\text{u}} = (u/u_{\text{lab}}) = (1 + x)^{-1} \tag{15}$$

where $x = V_{\text{rot.}}/u$. The plot pertains as well to the transformation of any individual velocity within a beam, supersonic or effusive, with the flow velocities u and u_{lab} replaced by V(with respect to source) → V(in laboratory).

The scanning capability of the rotating source is particularly useful for the study of collision processes, in the gas phase or with surfaces. Since interactions in the gas phase involve the relative velocity, the rotating source need not produce a low laboratory velocity. Instead, it can be scanned versus the fixed velocity of a stationary beam to cover a wide range of relative velocity. Using the rotating source in its speeding mode, augmented by seeding to further narrow the velocity spread, may prove most effective in achieving well-defined low relative velocities in such merged or crossed beam experiments.

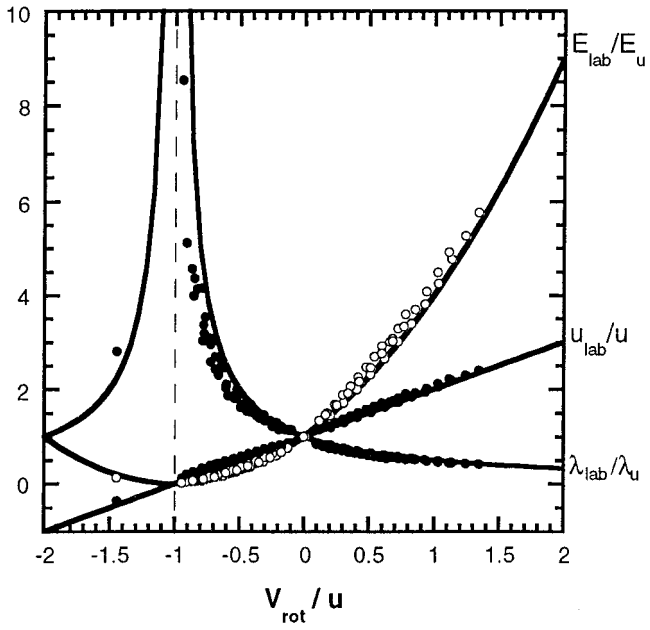

Figure 17. Reduced variable plot for rotating supersonic beams, enabling estimates of laboratory flow velocity, translational kinetic energy, and deBroglie wavelength as functions of the peripheral velocity of the rotor. E_{lab} and λ_{lab} correspond to $u_{\text{lab}} = u + V_{\text{rot.}}$; E_{u} and λ_{u} correspond to u. Points are from data of Figure 8 for rare gas beams.

A similar strategy may provide a means to trap product molecules from chemical reactions. Under single-collision conditions, a product molecule is born with a laboratory velocity given by a vector sum, $\mathbf{C} + \mathbf{U}$, where $\mathbf{C}$ denotes the velocity of the center-of-mass of the collision partners and $\mathbf{U}$ the recoil velocity of the product relative to the centroid. If counter-propagating reactant beams are directed into a trapping region,[43] and the velocity of one or both of the reactants adjusted to make $\mathbf{C} \approx -\mathbf{U}$, the product molecule will emerge with a very low laboratory velocity.[16] Since the products have a range of $\mathbf{U}$, the fraction rendered slow enough to trap in this fashion is small. However, the ease of scanning provided by the rotor permits this to be enhanced by optimizing the cancellation overlap between the centroid and recoil distributions.

Acknowledgment. We dedicate this paper to Harold Johnston, with admiration and gratitude for his creativity, architectural vision, and intrepid leadership in research, teaching, and public service. We are grateful for support received at the outset of this work from the Research Corporation and from the Milton Fund of Harvard University, and continuing support from the National Science Foundation.

References and Notes

(1) Stern, O. *Z. Phys.* **1920**, *2*, 49; *3*, 417. See: Ramsey, N. F. *Molecular Beams*; Oxford University Press: New York, 1956; p 21.
(2) Bull, T. H.; Moon, P. B. *Discuss. Faraday Soc.* **1954**, *17*, 54.
(3) Moon, P. B.; Rettner, C. T.; Simons, J. P. *Faraday Discuss.* **1977**, *77*, 630.
(4) Moon, P. B. *Proc. R. Soc. London A* **1978**, *360*, 303, and references cited therein.
(5) Gupta, M.; Herschbach, D. *J. Phys. Chem. A* **1999**, *103*, 10670.
(6) Katz, D. P. *J. Chem. Phys.* **1997**, *107*, 8491, and references cited therein.
(7) Seideman, T. *J. Chem. Phys.* **1997**, *106*, 288l; *107*, 10420, and references cited therein.
(8) Friedrich, B. *Phys. Rev. A* **2000**, *61*, 02543.
(9) Doyle, J. M.; Friedrich, B. *Nature* **1999**, *401*, 749.
(10) Metcalf, H. J.; van der Straten, P. *Laser Cooling and Trapping*; Springer: New York, 1999.

(11) Weinstein, J. D.; deCarvalho, R.; Guillet, T.; Friedrich, B.; Doyle, J. M. *Nature* **1998**, *395*, 148.

(12) Bethlem, H. L.; Berden, C.; Crompvoets, F. M. H.; Jongma, R. T.; van Roij, A. J. A.; Meijer, G. *Nature* **2000**, *406*, 491.

(13) Beijerinck, H. C. W.; Verster, N. F. *Physica* **1981**, *111C*, 327.

(14) Klots, C. *J. Chem. Phys.* **1980**, *72*, 192.

(15) Miller, D. R. In *Atomic and Molecular Beam Methods*, Vol. I.; Scoles, G., Ed.; Oxford University Press: New York, 1988; p 14.

(16) Gupta, M. Ph.D. Thesis, Harvard University, 2000.

(17) Pauly, H. In *Atomic and Molecular Beam Methods*, Vol. I.; Scoles, G., Ed.; Oxford University Press: New York, 1988; p 83.

(18) Beams, J. W. *Rev. Mod. Phys.* **1938**, *10*, 245.

(19) In principle, a further centrifugal effect can occur for a supersonic expansion, for which (in contrast to effusive flow) collisions persist for some distance beyond the exit nozzle. The centrifugal force should continue to act until such collisions become unimportant. Molecules in a supersonic expansion are accelerated from rest to their final flow velocity within a few nozzle diameters beyond the exit. An approximate calculation shows that the significant parameter is the ratio of this distance to R_{out}, of the order of or less than 1%. That provides an estimate of X_1/X, the ratio of the transverse velocity component imparted by the centrifugal force to the flow velocity. Thus, this effect can be disregarded.

(20) Even for $V_{rot.}$ up to 600 m/s (about the breaking limit for our rotor), a velocity of only about 2 m/s is enough to escape swatting; this corresponds to $E_{min} = 1$ mK. Swatting therefore becomes inconsequential for molecules directed slightly away from the rotor orbit.

(21) Kennard, E. H. *Kinetic Theory of Gases*; McGraw-Hill Book Co.: New York, 1938.

(22) Levine, R. D.; Bernstein, R. B. *Molecular Reaction Dynamics and Chemical Reactivity*; Oxford University Press: New York, 1987; p 84.

(23) Kramer, H. L.; Herschbach, D. *J. Chem. Phys.* **1970**, *53*, 2792.

(24) This configuration was employed in most runs. Another had $L_1 = 7$ cm, $L_2 = 17$ cm, with the same slit widths; this was used for the experiments shown in Figures 7−10 as well as the SF_6 and speeding mode runs in Figure 12. In both configurations, the second skimmer defines the beam transmitted to the detector; thus, for intensity calculations pertaining to eq 7, the parameters are as follows: $\sigma_s = 0.079$ cm^2; $\Omega = 2 \times 10^{-4}$ sr; $\Delta\theta = 16°$; so $\tau = 0.044/\omega$ and $G = \omega\tau\sigma_s = 0.0035$ cm^2.

(25) Fast ion gauge: Beam Dynamics, Inc., Eden Prairie, MN.

(26) Quadrupole mass spectrometer: ABB Extrel, Pittsburgh, PA.

(27) AC induction motor: Precision Drive Systems, 128 Durkee Lane, Dallas, NC 28034.

(28) Nonvolatile vacuum grease: Kluber Lubrication, Londonderry, NH.

(29) To prevent the motor from overheating, the manufacturer recommended running water through the housing and around the stator. Due to slight leakage in the internal seals of the motor, this cooling method was not feasible in our vacuum chamber, so we bolted the motor onto a water-cooled copper plate. However, if run too long at high speed, the rotor gradually heats due to friction (with the stationary inlet needle as well as in the spindle's ball bearings). To minimize this, data were taken in batches between "rest periods" in which the rotor was allowed to coast at low speed. The rotor temperature was monitored by observing the TOF spectrum of a Xe beam. To avoid overheating, we operated the motor at $\omega < 700$ rps, much below the rated maximum of 1333 rps. It would be better to circulate a low vapor pressure vacuum oil through the motor housing.

(30) PEEK: Scientific Instrument Services Inc., Ringoes, NJ.

(31) Glass capillary array: Burle Electro Optics, Sturbridge, MA. The number of active channels may be estimated from the area of the hole in the rotor (5.7 mm^2) divided by the cross-sectional area of the channel (7.8×10^{-5} mm^2) divided by 2 (for 50% transparency); this gives ~36 500 channels.

(32) Press, W. H.; et al. *Numerical Recipes in FORTRAN*, 2nd ed.; Cambridge University Press: Cambridge, U.K., 1992.

(33) Braker, W.; Mossman, A. L. *Matheson Gas Data Book;* Matheson Gas Products: NJ, 1980.

(34) The broadening of Δv for rotating seeded beams is in part artificial, due to scattering from the background gas exacerbated by the leaky inlet and centrifugal enhancement of carrier gas flow. Beyond that, however, the theory of inverse seeded supersonic beams[15] involves complications that may accommodate this broadening. In particular, increases in the seeding mole fraction caused by deviations from equilibrium flow within the rotor or from centrifugal fractionation would be expected to produce higher parallel temperatures for the seeded molecule.

(35) Loesch, H. J. *Chem. Phys.* **1996**, *207*, 427.

(36) Ye, J.; Ma, L.; Hall, J. L. *J. Opt. Soc.* **1998**, *15*, 6. Ye, J. Private communication.

(37) Ghaffari, B.; Gerton, J. M.; McAlexander, W. I.; Strecker, K. E.; Homan, D. M.; Hulet, R. G. *Phys. Rev. A* **1999**, *60*, 3878.

(38) Parameters for beam flux distributions: for PS, $u = 715$ m/s, $\Delta v = 152$ m/s, $C = 1.28 \times 10^8$; for ISS, $u = 319$ m/s; $\Delta v = 43$ m/s; $C = 4.72 \times 10^9$; for MCE, $\alpha_o = 383$ m/s; $C = 6.1 \times 10^5$. For PS, the centrifugal enhancement of eq 8 was included (it grew to a factor of 140 for $V_{rot.} = 850$ m/s); for ISS and MCE it was negligible. Note that, at the low kinetic energies considered here, eq 12 is a crude approximation (omitting glory and orbiting resonance structure, cf. ref 22) but adequate for the rough estimating of attenuation by collisions.

(39) Stwalley, W. C.; Wang, H. *J. Mol. Spectrosc.* **1999**, *195*, 194. Bahns, J. T.; Gould, P. L.; Stwalley, W. C. *Adv. At. Mol. Opt. Phys.* **2000**, *42*, 171.

(40) Stapelfeldt, H.; Sakai, H.; Constant, E.; Corkum, P. *Phys. Rev. Lett.* **1997**, *79*, 2787.

(41) Zhigilei, L. V.; Kodali, P. B. S.; Garrison, B. J. *J. Phys. Chem. B* **1998**, *102*, 2845, and references cited therein.

(42) Karas, M. *Biochem. Mass Spectrom.* **1997**, *14*, 897.

(43) Brinkman, C.; Loesch, H. J. *Workshop on Prospects for Cold Molecules;* Max-Planck Institute für Kernphysik: Heidelberg, Grermany, 1999 (Nov).